Computer Simulation of High-Speed Spinning of PET*

JEFFREY S. DENTON, JOHN A. CUCULO,† and PAUL A. TUCKER

Department of Textile Engineering, Chemistry, and Science, College of Textiles, North Carolina State University, Raleigh, North Carolina, 27695-8301

SYNOPSIS

An interactive computer simulation of the steady-state melt spinning of poly(ethylene terephthalate) was developed based upon a combination of physical laws and empirical relationships. The simulation incorporates crystallization effects which makes it valid for a wide range of take-up speeds. Modifications to the conventional threadline that allow judicious control over the threadline dynamics were modeled and included in the simulation for exploration of the effects of these perturbations. The modifications include quenching and on-line zone heating. The simulation was verified using experimental measurements of threadline diameter, velocity, and temperature at 3000, 4000, 5000, and 6000 m/min take-up. Off-line measurements of crystallinity and birefringence were also compared with the values calculated by the simulation at these speeds. © 1995 John Wiley & Sons, Inc.

THEORETICAL CONSIDERATIONS

Three major equations govern the melt spinning process. They follow from the general conservation laws of physics. These are the mass balance, the force balance, and the energy balance.

The mass balance, or the continuity equation, follows from the conservation of mass. Therefore, the mass per unit time of the fiber is constant along the threadline. Mathematically, this is[1]

$$W = \rho A v$$

where W = mass throughput, ρ = fiber density, A = fiber cross-sectional area, and v = fiber velocity. This equation is essential in deriving the equations that follow and will be extensively substituted for undefined variables. For a given throughput, the fiber velocity or the cross-sectional area can be calculated from the mass balance, provided the other two variables are known.

The development of the equations necessary to model the melt spinning process begins with a force balance along the threadline. The force balance on the threadline is as follows[2]:

$$F_{\text{rheo}} + F_{\text{aero}} + F_{\text{ln}} + F_{\text{sun}} = F_{\text{ext}} + F_{\text{grav}}.$$

These terms describe the contributions of the rheological force, aerodynamical drag, inertia, surface tension, external force from the take-up device, and gravity, respectively.

The rheological force, F_{rheo}, is the force that acts to deform the polymer. It is a measure of the material's resistance to flow. At the spinneret face, this is the only source of tension. To analyze F_{rheo} should consider a differential slice of the threadline, where two normal stresses are revealed. One acts normal to the threadline cross section, designated zz, and the other acts normal to the surface of the fiber, xx. zz is created when a force is applied in the z direction. xx is associated with the decrease in diameter when an object is placed in tension (assuming constant volume). Thus xx is a result of axial force. Die swell effects are ignored, and the initial diameter of the filament is assumed to be the diameter of the orifice. Therefore, mathematically, the tensile stress on a cylindrical body in these coordinates is given by

$$\tau = \tau_{zz} - \tau_{xx}$$

and the force associated with this tensile stress is given by

$$F_{\text{rheo}} = \frac{\pi D^2}{4}(\tau_{zz} - \tau_{xx})$$

* This article is based on the thesis of Jeffrey S. Denton, North Carolina State University (1993).

† To whom correspondence should be addressed.

Journal of Applied Polymer Science, Vol. 57, 939-951 (1995)
 CCC 0021-8995/95/080939-13

where D is the fiber diameter.

F_{aero} is the frictional air drag on the fiber. This force is cumulative over the length of the threadline so it appears as the integral

$$F_{aero} = \int \pi D C_f \rho_a \frac{v_{rel}^2}{2} dz$$

where Ddz = fiber surface area increment, C_f = coefficient of friction, ρ_a = density of air, $v_{rel} = v - v_a \cos \phi$, v_a = velocity of air, and ϕ = angle of air flow on the threadline. The drag coefficient, C_f, is a function of fiber velocity and has been reported as an empirical function by several sources. The equation used for this simulation is presented by Matsui[3]:

$$C_f = 0.347 \, \mathrm{Re}_d^{-0.61}.$$

Re_d is the Reynolds number of the air relative to the fiber diameter, d, defined as

$$\mathrm{Re}_d = \frac{D v_a}{\nu_a}$$

where D is the diameter of the fiber, v_a is the air velocity, and ν_a is the kinematic viscosity of the air, defined as

$$\nu_a = \frac{\eta_a}{\rho_a}$$

where η_a is the dynamic air viscosity and ρ_a is the density of the air. The properties of air, thermal conductivity, density, and viscosity, are reported by Gagon[4] as functions derived from data published by Krieth[5]:
thermal conductivity,

$$K_f = 4.134 \times 10^{-3}(3.79 \times 10^{-5} \, T^{0.9} + 0.013)$$

density,

$$\rho_a = 1.1383 \times 10^{-3}\left(\frac{560}{460 + T}\right)$$

and viscosity,

$$\eta_a = 1.49 \, 10^{-4}(1.7 \, 10^{-3} \, T - 1 \, 10^{-12} \, T^4 + 1.11)$$

where T in each case is temperature in °F.

It has been observed[2] that normally for long exposed sections of the threadline, air drag force is higher that any other force contributing to the spinning tension. Thus, practically all tension at the end of the filament is controlled by air drag. This is important especially in high-speed spinning where the take-up speeds, on which the air drag is dependent, exceed 3000 m/min. The transition from low-speed spinning to high-speed spinning is a transition from a process in which the spinning tension is controlled by the material in the form of rheological force to one where the threadline tension is controlled mechanically by air drag and inertial effects.

Inertia contributes to the total tension in a region in the threadline above the point where air drag dominates. It is represented as

$$F_{in} = W(v - v_0)$$

where v_0 is the initial fiber velocity.

The forces due to gravity and surface tension are generally small compared with the contributions from the others. Therefore these forces will be disregarded in the force balance.

The external force placed on the threadline is a constant depending upon the method of take-up. External force is supplied by the take-up device operating at a constant speed. The external force is a resultant force, decided by the other forces along the threadline.

The accumulation of energy along the threadline has major influences from two sources, convective heat loss and heat gained from crystallization. Radiation and conductive heat loss are small compared to convective and crystallization effects and will be ignored in this simulation.

Convection is the process by which heat is transferred through a fluid between objects of different temperatures. In fiber spinning, the two objects are the fiber and the ambient air, and the convective fluid is the air surrounding the fiber. The heat loss due to convection is described as

$$\frac{-\pi D h}{W C_p}(T - T_a)$$

where D = fiber diameter, h = heat transfer coefficient, C_p = polymer specific heat, T = fiber temperature at a point z along the threadline, and T_a = ambient air temperature. The heat gained by the fiber due to the crystallization of the polymer along the threadline during the spinning process is described as

$$\frac{\Delta H}{C_p} \frac{dX_c}{dz}$$

where ΔH is the polymer heat of fusion. So the energy balance takes the form[13]

$$\frac{dT}{dz} = \frac{-\pi Dh}{WC_p}(T - T_a) + \frac{\Delta H}{C_p}\frac{dX_c}{dz}.$$

Kase and Matsuo[6] reported a correlation combining the effects of cross-flow and parallel flow of air on the cooling process. Breaking the correlation into its vector components, for parallel flow, the relationship is given by

$$\mathrm{Nu} = 0.42\ \mathrm{Re}_d^{0.334}$$

and, for cross-flow, the relationship is given by

$$\mathrm{Nu} = 0.746\ \mathrm{Re}_d^{0.38}$$

where Nu = Nusselt number, Nu = hD/K_f, and K_f = thermal conductivity. Kase and Matsuo[7] later expanded their relationship to combine cross- and parallel flow into a function in terms of the fiber velocity and the cross-flow air velocity:

$$\mathrm{Nu} = 0.42\ \mathrm{Re}_d^{0.334}\left[1 + \left(8\frac{v_a}{v}\right)^2\right]^{0.167}$$

where v_a is the velocity of the cross-flow air.

The physical visualization of the rheological behavior of a fluid is made by considering the material to be mechanical elements that represent the observed behavior of the material. Four different models for the behavior of the polymer are to be included in the simulation. These are the Newtonian model, the Maxwell model, the Phan–Thien model, and the power-law model.

A Newtonian liquid is represented by a dashpot consisting of a container filled with a viscous liquid. A piston is placed in the container and is acted upon by a stress. All turbulence, gravitational, inertial, and end effects are considered negligible. The force applied to the piston exerts a stress on the fluid that shears at a constant rate. Therefore if the force is doubled then the shearing rate and the rate at which the piston rises in the fluid is doubled. The piston has no tendency to return to its original position if the force is removed. This system exhibits pure Newtonian behavior: the relationship between the shear stress and the shear rate is linear and the system has no "memory" or preferred form. Mathematically this is written[8]

$$\tau = \eta\frac{dv}{dz}$$

where dv/dz is the velocity gradient, or shear rate, in the z direction, τ is the stress and the proportionality constant, η, is the viscosity of the material.

The Maxwell model consists of an ideal spring in series with a dashpot. When a force is applied, the spring immediately elongates and the same stress is carried to the dashpot, within which the piston moves at a constant rate if the applied stress is constant. Therefore the total deformation is the sum of the deformation of the components, and the rate of deformation is equal to the sum of the individual rates:

$$\frac{d\gamma_{\mathrm{total}}}{dt} = \frac{1}{G}\frac{d\tau}{dt} + \frac{\tau}{\eta}$$

where G is the modulus of the spring.

The Phan–Thien model[9] is a nonlinear constitutive equation for polymer melts and concentrated solutions based on a Lodge–Yamamoto[10–14] type of network theory. Network junctions are assumed to behave nonaffinely in a well-defined manner. Good agreement is shown between the theory and all data examined, including melt spinning.

Assuming only axial (zz) and radial (rr) stresses, and restricting the analysis to one relaxation time, the Phan–Thien constitutive equations are[9]

$$K\tau_{rr} + \lambda\left(v\frac{d\tau_{rr}}{dz} + \frac{dv}{dz}\tau_{rr}\right) = -G\lambda\frac{dv}{dz}$$

and

$$K\tau_{zz} + \lambda\left(v\frac{d\tau_{zz}}{dz} + 2\frac{dv}{dz}\tau_{zz}\right) = 2G\lambda\frac{dv}{dz}$$

where $K = \exp[E/G(2\tau_{rr} + \tau_{zz})]$, λ = relaxation time, and E = a fitting parameter, 0.015. The comparison of experimental data to the Newtonian model led researchers to develop the power-law model. Although the Newtonian assumption qualitatively predicts the behavior of some fluids, a more quantitative fit was sought. Slight deviations from Newtonian behavior are described by the following modification:

$$\tau = K\left(\frac{dv}{dz}\right)^n$$

where K is known as the consistency index and n is the flow behavior index. In spite of its simplicity, the power-law equation gives surprisingly good results, describing non-Newtonian behavior in the simplest mathematical form.

The crystallization process may be divided into two processes, namely nucleation and crystal growth. Nucleation is the initiation of a small amount of crystalline material. There are three different types of nucleation that can occur in polymer melts. Heterogeneous nucleation occurs when there is a second phase present in the polymer melt. This second phase could be an impurity or a nucleating agent which has been added to the melt to instigate crystallization. Nucleation occurs at the interface between the two phases. Homogeneous nucleation is the spontaneous aggregation of the polymer molecules into an ordered array. This aggregation is considered to be reversible by thermal motion. Without the influence of external stresses, however, this type of nucleation seldom actually occurs. Nucleation can also be influenced by molecular orientation. This follows from the homogeneous nucleation because nucleation is enhanced by molecular alignment. These regions of orientation can easily be converted into nuclei. Such orientation can be achieved through shear stress or tensile stress. This type of initiation is known as stress-induced crystallization.

The driving force behind nucleation is provided by the Gibbs' free energy of the transformation of kinetics elements into a crystalline cluster.[15] The bulk free energy is a function of temperature, enthalpy, and entropy. Usually a linear approximation is assumed:

$$\Delta f = \Delta h - T\Delta s = \Delta h \frac{T_m - T}{T_m}$$

where f = free energy, h = enthalpy, s = entropy, T = temperature, and T_m = critical transition temperature. The free energy is negative only when the temperature lies below the critical transition temperature. Thus, in the case of homogeneous nucleation, the amount of supercooling is the controlling factor. Molecular orientation, however, due to the levels of stress in the spinning threadline, affects the entropy of the system. Orientation of the melt decreases its entropy as compared with the unoriented melt and the entropy change corresponding to the transition from the melt to a crystal is decreased. Therefore, at a given degree of supercooling, the free energy associated with the transition is decreased. In physical terms, the orientation of the chains in the melt brings them close to the alignment eventually found in the crystalline state and thus makes crystallization easier.[16]

The advent of high-speed take-up capabilities resulted in the ability to form semicrystalline, highly oriented PET fibers without the need for the postdrawing process. At speeds above 4000 m/min there is apparently sufficient orientation in the molecules to induce crystallization. Some supercooling, however, is still required to drive this process. The structure of the crystalline regions in fibers is still not generally agreed upon. X-ray evidence indicates that the molecules are aligned and that a long periodicity is present. This would suggest a lamellar structure with disordered phases can be found between the crystalline regions, but the width of the lamellae is uncertain. However, evidence has been presented[17–20] indicating that the crystals are in fact fibrillar in nature, with the fibrils and the polymer chains collinear with the macroscopic axis. The stress in a high-speed threadline asserts itself to a narrow zone of instability not far from the spinneret. This transition zone resembles "necking" commonly seen in plastic deformation of solids, such as in the postdrawing process. It is this necking phenomena that holds the key to the transition from an essentially completely amorphous fiber to one with semicrystalline fibrillar structure.

It is still not certain what role the neck formation plays in the onset of crystallization. One theory is that the formation of the neck, and therefore the decrease in diameter, increase in local stress, and the stress-induced orientation of the molecules triggers the crystallization process.[21,22] Also possible is the opposite effect.[23] Crystallization results in a denser, more ordered, and stable system; therefore the diameter is capable of attenuating between the crystallized region and the uncrystallized, upstream region. Also the heat produced by the crystallization process can result in a lowering of the viscosity of the fiber, facilitating drawing and diameter reduction over a short range.

The crystallization within the spinning threadline is described using the relationship proposed by Nakamura, et al.[24] In its differential form, the equation is

$$\frac{dX(t)}{dt} = KX_{\max}(1-\theta)\left[\ln\left(\frac{1}{1-\theta}\right)\right].$$

The energy equation uses the crystallization position gradient whereas the equation from Nakamura et al. describes crystallization with the time gradient. Using the chain rule the time gradient is converted to the position gradient:

$$\frac{dX}{dt} = \frac{dX}{dt}\frac{dt}{dz}$$

and

$$\frac{dz}{dt} = v$$

Making this substitution the crystallization equation is obtained:

$$\frac{dX(t)}{dz} = \frac{KX_{\max}}{v}(1-\theta)\left[\ln\left(\frac{1}{1-\theta}\right)\right].$$

Katayama and Yoon[25] postulated the following expressions for the crystallization rate constant:

$$\frac{k_{a0}}{k_a} = \exp\left[\frac{1.2\ 10^6}{(T+273)(300-T)}\left[\times\left(1-\frac{1}{1+160(\Delta n)^2\dfrac{T+273}{300-T}}\right)\right]\right]$$

and

$$k_a = \exp\left[9.34 - \frac{682}{T-43} - \frac{4.53\ 10^5}{(T+273)(300-T)}\right].$$

Birefringence is reported as a function of temperature and stress from Katayama and Yoon[25] as

$$\Delta n = 0.2\left(1-\exp\left[\frac{-1.65\ 10^{-6}\tau}{T-273}\right]\right),$$

who found that the stress-optical law[26] did not hold well for the high levels of stress found in the high-speed threadline.

EXPERIMENTAL

Poly(ethylene terephthalate) (PET) used in this study was supplied in chip form by Goodyear Tire and Rubber Company. The chips are approximately 4 × 2 mm in size and intrinsic viscosities (IV) of 0.57 and 0.95 were available. The number average molecular weights of these resins are 17,286 for the low IV chip, and 36,615 for the high IV chip.

The polymer chips are typically dried overnight in a vacuum oven at a temperature of 140°C. Before transferring the chip to the hopper the extruder is heated. Extrusion begins with specially formulated thermally stable polypropylene that flushes the extruder before and after all spinning operations. Before experimental runs, the extruder is typically heated for approximately 3 h to the desired temperature profile. Once the extruder has reached the desired temperature, and the temperature has stabilized, the vacuum oven is purged with nitrogen. The chips are transferred to the chip hopper, where they remain blanketed by nitrogen throughout operation of the extruder. After approximately 45 min of operation, the extruder will be completely depleted of the polypropylene and the resulting PET filament is ready to be taken up on the godet roll (Fig. 1).

A hand aspirator collects the extruder filament and helps place it on the spinning godet. String-up is achieved by manually wrapping the fiber around the godet using the aspirator. Often it is necessary to wind up the filament at a low speed and then increase the speed of the roll to the desired take-up speed. Once a stable threadline is established, on-line measurements can commence.

Although there are several variables in the melt spinning simulation that could be compared with experimental data, limitations exist in the availability of instruments to measure these variables. Also care must be exercised in the manner that these data are obtained. Experimental measurement must not disturb the threadline. Any disturbance can alter

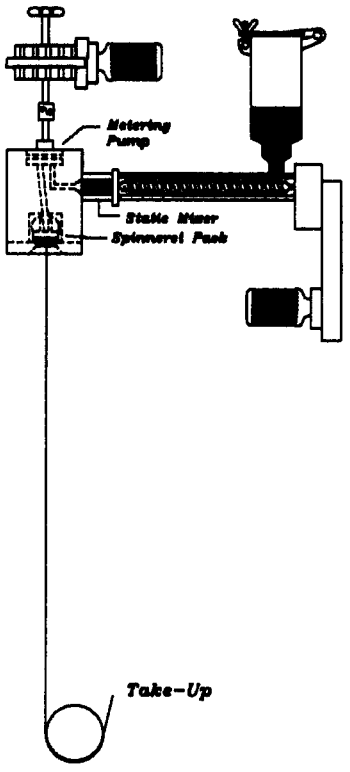

Figure 1 Melt spinning system.

the physical properties of the spinning fiber and thus skew the results. Noncontact measurement of threadline variables is essential to obtain data that would be suitable for comparison with data from the simulation.

Three noncontact devices are available for the measurement of threadline properties: the Zimmer diameter monitor, for threadline diameter measurement; a laser Doppler anemometer (LDA), loaned from an industrial source for threadline velocity measurement; and an infrared temperature measuring device, also lent for experimentation from an industrial source.

The Zimmer diameter monitor (Model 460A/2, Zimmer OHG, Germany) was originally developed for monitoring and controlling diameters in the wire extrusion process. The system consists of a sensing head connected to a digital readout. The device can measure diameters up to 2 mm. Measurement of the diameter of the target is obtained using a backlighting technique where the sensor in the head returns the amount of light detected from the source as a percentage of the total. While this technique works well for opaque targets, problems exist when measuring a fiber, which can be translucent.

A calibration curve was developed by first setting the instrument gain at a little less than full gain to avoid any noise that might be incurred due to amplifier saturation. Then, for each fiber in the calibration wheel, the measured diameter was compared with the actual diameter, as measured by microscopy. The result is a curve from which an equation can be obtained to calculate the actual diameter of a fiber. The equation was generated using a least-squares best-fit statistical approach.

Because the axial movement of the fiber as it is spinning is at times large, direct measurement of the diameter was difficult. Therefore, the device was coupled with a computer to facilitate large sampling of the filament diameter. One thousand samples could be obtained in a relatively short time and the actual diameter was assumed to be the most frequently occurring because there was an obvious modal value. The calibration equation was incorporated within the software to calculate the actual fiber diameter from the data collected.

Threadline velocity profiles can be measured using the LDA. This device consists of a laser mounted in parallel with a photomultiplier tube and is controlled by a processor that performs counting functions during velocity measurements. Through mathematical manipulation, a velocity can be calculated.

The device was interfaced with a computer to aid in the acquisition and analysis of the data. Large data sets could be collected and subsequently analyzed statistically for the mean weighted value. The velocity was measured at various points along the threadline, usually every 10 cm, and the mean value of the collected data was assumed to be the velocity at each point.

The software allows for complete control of the experiment, including adjustment in the total number of samples to be collected, the time frame within which the samples were to be collected, and provides statistical analysis of the samples, as well as graphical indication of the sample sets. Both weighted and unweighted mean values can be determined, and the software will calculate standard deviation and skewness of the sampled data. The weighted average of the samples is assumed to be the velocity of the fiber assuming the standard deviation was within acceptable values.

No specific details are available concerning the internal operation of the infrared temperature measuring device, for it is still considered proprietary by the company that loaned it. The device is an infrared-based system, using a background target heated to a specific temperature. The sensing head was mounted on a stand that provided manipulation of the device in all directions. The temperature of the target was measured by thermocouple. The control panel of the device included a small monochrome monitor on which a trace of the target area was displayed. On this display a flat plateau indicated the target block, and, when the fiber was in position in front of the target block, it was evident as a peak or dip, indicating that the temperature of the fiber was hotter or colder, respectively, than that of the target block. By adjusting the temperature of the block appropriately, the peak or dip could be eliminated. When no peak or dip could be distinguished it was assumed that the block temperature and the fiber temperature were the same. The device was limited in the range of temperatures that could be measured with confidence. The cooler the fiber, the less accurate the indicated temperature became. The infrared sensors were cooled with liquid nitrogen. Thus the device operated best when the greatest temperature difference between the target and the sensing head was maintained.

Verification

A simulation is useless if it cannot be used with a degree of confidence obtained only from verifying the results of the simulation with experimental data taken from the actual process. Validity of the simulation is more important than any theoretical considerations that might be used in developing the

Table I Experimental Threadline Parameters

Figure No.	Take-Up Speed (m/min)	Melt Temperature (°C)	Denier	IV	Zone Quench	Zone Heat
2	5000	295	5	0.6	None	None
3	6000	295	5	0.6	None	None
4	4000	295	7.5	0.6	200 fpm, 25°C	None
6	5000	295	5	0.6	None	5 cm, 250°C
7	6000	295	5	0.6	None	5 cm, 250°C
8	5000	295	5	0.6	None	None
9	5000	295	5	0.6	None	5 cm, 250°C
10	6000	295	5	0.6	None	5 cm, 250°C
11	5000	300	5	0.95	None	shroud @295°C
12	Various	295	5	0.95	None	None

mathematical relationships that form the simulation. Without it, the success of the model cannot be determined. Diameter measurements were made on several threadlines of various take-up speeds and, unless otherwise indicated, each was a five-denier filament spun at 295°C. Early experimentation confirmed that the assumption of Newtonian behavior would be sufficient in describing the behavior of the PET threadline. Thus all subsequent data from the simulation were calculated using the Newtonian model. The parameters for each spinning trial are presented in Table I. Figure 2 shows the comparison of experimentally measured threadline diameters with those calculated by the simulation at 5000 m/min take-up speed. The experimental points fit closely with the calculated curve for this threadline. At 6000 m/min (Fig. 3) the simulation reaches its final diameter at approximately 30 cm closer to the spinneret face than do the measured values.

To establish the validity of the quench model incorporated by the program, diameter measurements were taken at various quench air speeds. Figure 4 shows the effect of 200 ft/min quenching on a 4000 m/min threadline. Because the area being quenched by the chamber lies well above the area where the measurements were made the trend is similar to the previous figure.

One of the interesting aspects of modifying the threadline dynamics is the apparent improvement in operability in the spinning operation when using the heated chamber close to the spinneret (Fig. 5). Thus the verification of the model for the heating chamber is important. At 5000 m/min take-up (Fig. 6) the experimental data begin to indicate a slight

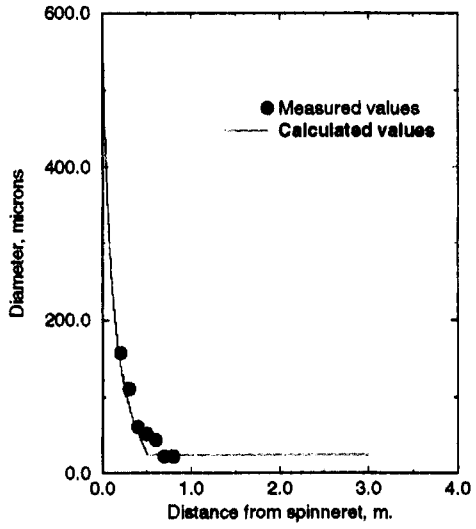

Figure 2 Comparison of measured and calculated threadline diameters at 6000 m/min take-up.

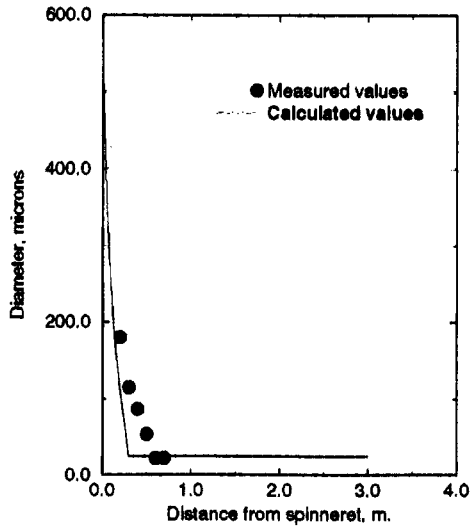

Figure 3 Comparison of measured and calculated threadline diameters at 6000 m/min take-up.

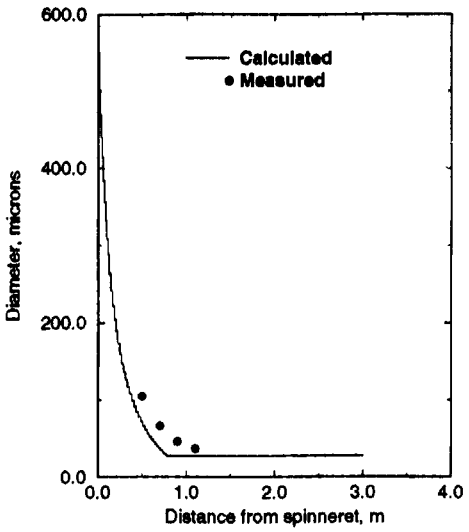

Figure 4 Comparison of measured and calculated threadline diameters at 4000 m/min, 7.5 denier, 200 ft/min quench.

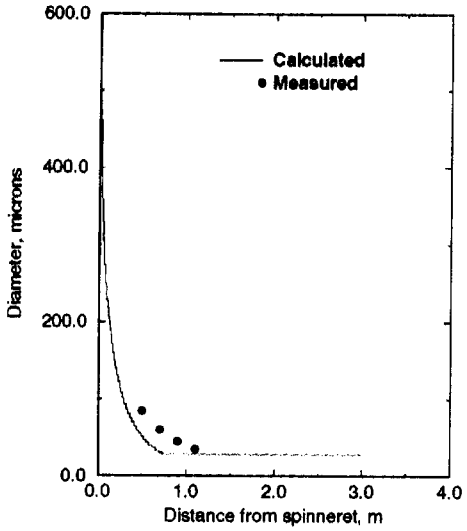

Figure 6 Comparison of measured and calculated threadline diameters at 5000 m/min take-up with OLZH at 5 cm, 250°C.

necking in the threadline, while the simulation fails to do so. Again there is a discrepancy of about 30 cm between the measured and calculated values, but the overall profiles are the same. The same discussion applies at 6000 m/min take-up (Fig. 7) where the rapid stress and velocity development as predicted by the simulation force the diameter profile to reach its final value well before the experimentally observed profile.

Velocity measurements were made on several threadlines of various take-up speeds for comparison with the simulation. Each threadline was a five-denier filament, spun at a melt temperature of 295°C, unless otherwise indicated.

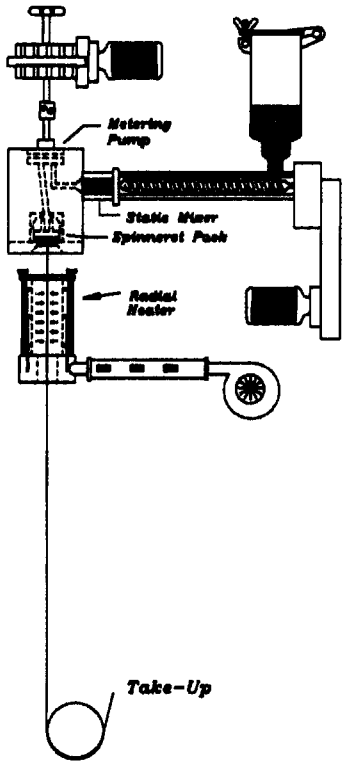

Figure 5 Melt spinning system with radial quench.

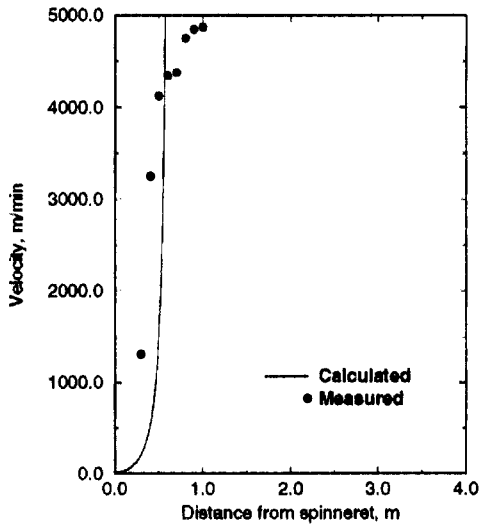

Figure 7 Comparison of measured and calculated threadline velocities at 5000 m/min take-up with OLZH at 5 cm, 250°C.

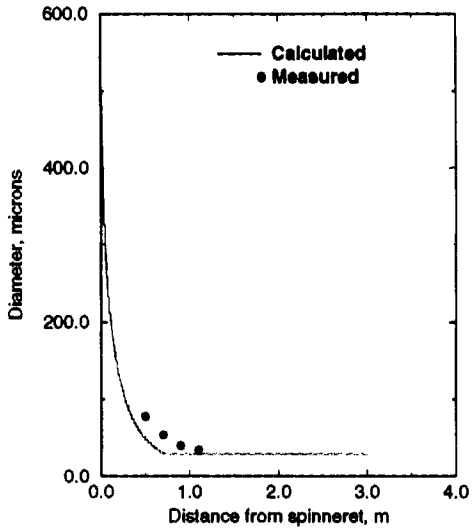

Figure 8 Comparison of measured and calculated threadline diameters at 6000 m/min with OLZH at 5 cm, 250°C.

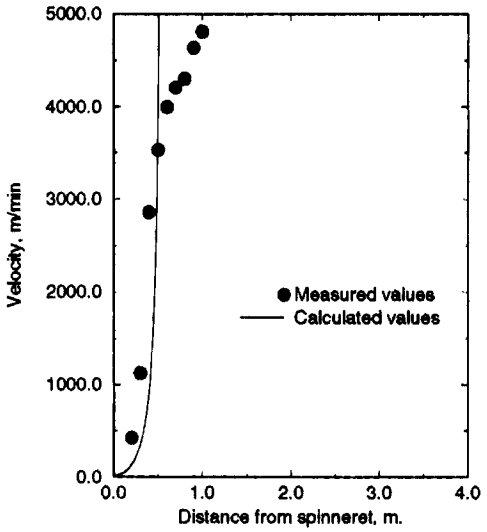

Figure 9 Comparison of measured and calculated threadline velocities at 5000 m/min take-up.

At 5000 m/min take-up (Fig. 8), the inflection point is not as evident and the predicted values fall close to the measured velocities. Velocity measurements were made in conjunction with the diameter measurements using the heated quench chamber near the spinneret face. At 5000 m/min (Fig. 9), the measured velocities are generally higher than the predicted at a given position on the threadline, reversing the expected trend. However, the values are very close to one another. An inflection point apparent in the measured data is not indicated by the simulation for this particular situation. At 6000 m/min take-up (Fig. 10), the predicted velocities are quite close to those measured, but again the simulation reaches its final value before the experimental termination point.

At 5000 m/min take-up, with the 0.95 IV polymer, the simulation predicts the occurrence of crystallization within the threadline, as evident by the large jump in temperature at a distance of about 25 cm from the spinneret face (Fig. 11). Because of the position of the heated shroud, no measurements could be made above 30 cm. The measured temperatures are higher than the calculated temperatures at each position. For comparative purposes, the simulated temperature profile with no heated sleeve is plotted as well. The curves are very similar, with the exception being an apparent delay in the onset of crystallization when the heated shroud is in place.

In an attempt to validate the two major empirical relationships found in the simulation, namely the crystallinity equation and the birefringence equation, data from Lin[27] was used to compare the predicted crystallinity levels and the predicted birefringence levels with data measured from fiber samples collected in the laboratory. The predicted values were taken from the output data file generated by the program. Samples of low IV and high IV PET are compared, each taken at various take-up speeds, ranging from 3000 to 6000 m/min.

The simulation does not predict birefringence well. The values are much lower than those measured experimentally. At 0.6 IV, the simulation

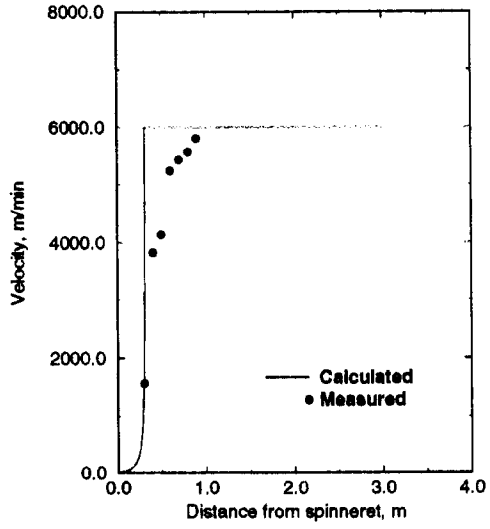

Figure 10 Comparison of measured and calculated threadline velocities at 6000 m/min take-up with OLZH at 5 cm, 250°C.

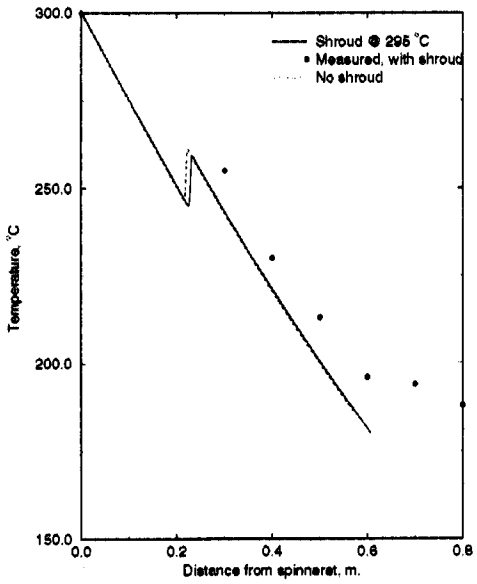

Figure 11 Temperature profile, showing the effects of the heated shroud, 5000 m/min, 0.95 IV polymer, shroud at 295°C, 13-cm length.

does not predict the occurrence of crystallization at any take-up speed. Experimentally PET fibers exhibit significant crystallinity at take-up speeds exceeding 4000 m/min. Figure 12 compares the predicted and measured level of crystallinity in the fiber for 0.9 IV polymer. The simulation predicts a level of crystallinity higher than that measured experimentally. The relationship describing crystallization is functional, but the accuracy is not sufficient without adjustment of the parameters in the equation.

Good agreement between the predicted and the measured values of diameter, velocity, and temperature is demonstrated. The diameter profiles are not as good as the velocity and temperature profiles, but overall the calculated profiles compare well with the experimental. Comparison with crystallinity and birefringence measurements made off-line on collected samples, however, point out deficiencies of the program in the prediction of these properties. Because the calculations are based on empirical relationships adapted from other work, this was somewhat expected. The great disparity between the program and the experimentally measured data at low IVs was not expected. Thus exploration of these relationships is warranted and caution is advised if the simulation is to be used for the prediction of these properties under the circumstances where the preceding analysis has shown it to be questionable.

Computer Experimentation

Initial experimentation with the simulation generated simple illustrative threadlines. An understanding of the dynamics of these typical threadlines is needed before delving into the more complicated issues of modifying the dynamics in such a way to improve or enhance the process. Historically the regions of interest when discussing threadline dynamics revolve around the increasing of the take-up speed, because it is with increasing take-up speed that most of the phenomena surrounding the spinning of PET are greatly increased in magnitude.

Threadline profiles for a high-speed take-up threadline are all quite similar in that each displays a dramatic increase in each parameter, almost in a step-function manner. Figure 13 illustrates this point. This figure shows the stress profile for a 6000 m/min threadline for a 0.6 IV polymer. The stress is negligible until a point in the threadline is reached where the stress increases rapidly to its final value. The final value is reached at less than 50 cm away from the spinneret face.

A gradual increase in the threadline velocity in the upper region of the threadline is shown in Figure 14, but again the velocity increases to its final value almost immediately. The simulation does not indicate any crystallization at this take-up speed and IV, which is a shortcoming because some crystallization is known to occur under these conditions.

The threadline temperature profile (Fig. 15) is the only profile at this speed to demonstrate the gradual exponential decay that would be expected.

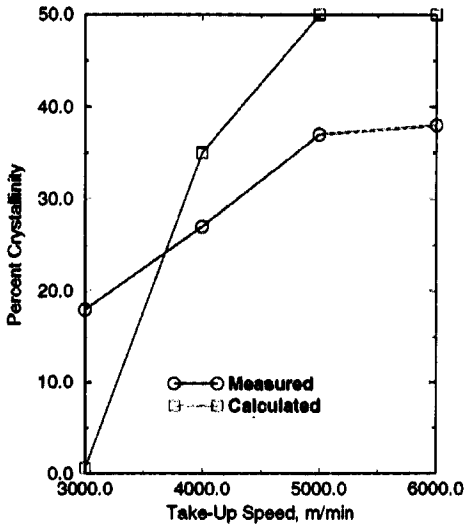

Figure 12 Comparison of crystallization, measured off-line vs. simulated, for 0.95 IV polymer at various take-up speeds.

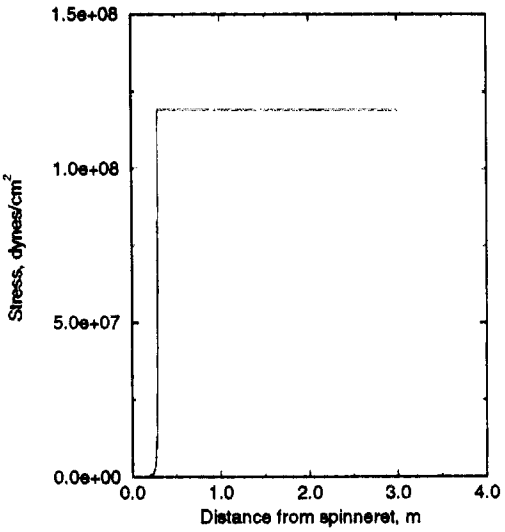

Figure 13 Stress profile for a 6000 m/min take-up threadline, 0.6 IV polymer.

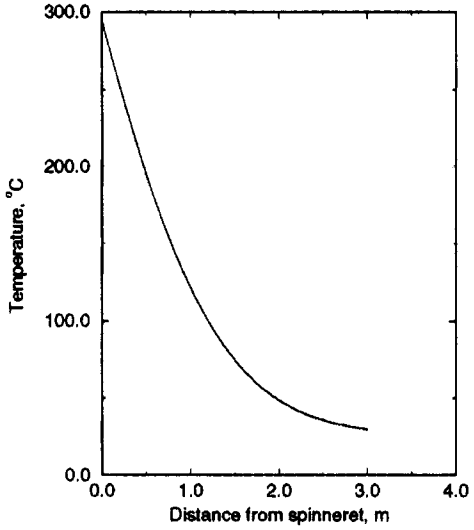

Figure 15 Temperature profile for a 6000 m/min threadline, 0.6 IV polymer.

The curve is smooth, again an indication that no crystallization occurs under these conditions. Had the fiber crystallized, a bump in the profile at the point of occurrence would have been apparent. While the simulation determined that no crystallization would occur, thus eliminating the possibility of necking, the diameter profile (Fig. 16) does indicate that the final diameter of the fiber is reached abruptly, in contrast to the profiles shown earlier for the lower take-up speeds. Although the difference is minimal, the profile does support the observed experimental threadline behavior at the higher take-up speeds. The diameter does not gradually reach its final value; in contrast, the value is reached suddenly at the freeze point in the threadline.

Figure 17, the birefringence profile, demonstrates the rapid structure development occurring in the high take-up speed threadline. Almost no orientation is indicated until the stress level begins to climb. Once this breakpoint is reached, the birefringence quickly increases to its final value.

At 6000 m/min take-up, there is little difference indicated for the incorporation of quench air in the stress profile. Evidently the stress levels are so dominated by the increased take-up speed that the slight cooling in the threadline afforded by the quench adds

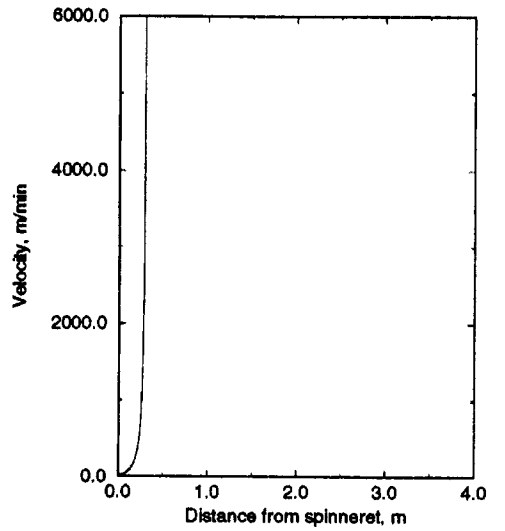

Figure 14 Velocity profile for a 6000 m/min take-up threadline, 0.6 IV polymer.

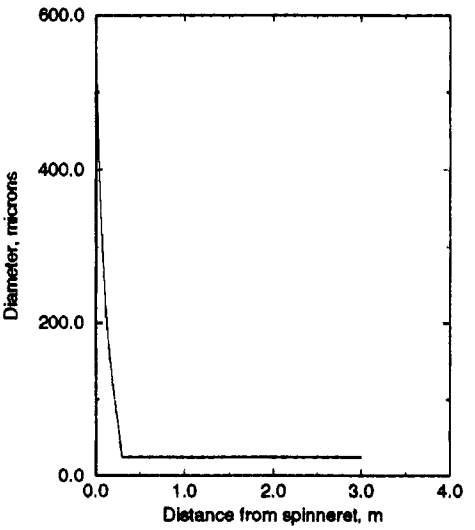

Figure 16 Diameter profile for a 6000 m/min take-up threadline, 0.6 IV polymer.

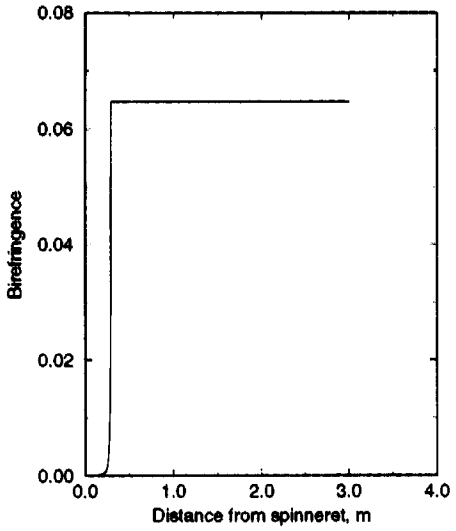

Figure 17 Birefringence profile for a 6000 m/min take-up threadline, 0.6 IV polymer.

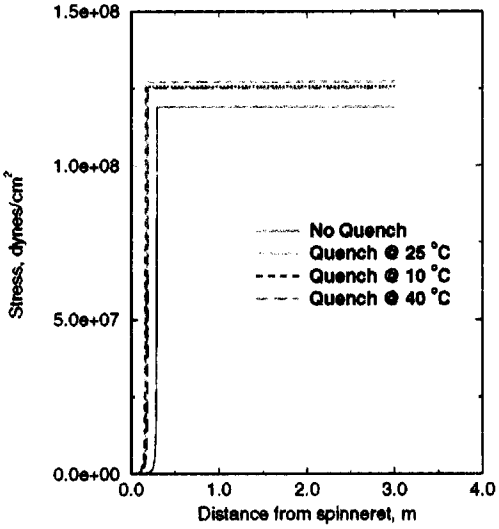

Figure 18 Stress profiles comparing the effects of quench air temperature at 6000 m/min take-up, 0.6 IV polymer.

very little. Thus the stress profile (Fig. 18) indicates that only a small increase in the overall threadline stress is gained through the use of quench air.

The program does indicate the presence of some crystallization in the threadlines where quenching is present. No crystallization is predicted when the threadline is not quenched, however, indicating that while the stress levels are increased only slightly when quenched externally, the amount is apparently sufficient to initiate the crystallization process.

Quench air effects are apparent in the temperature profile (Fig. 19) calculated for these conditions. The fiber cools more rapidly under the influence of the quenching air, due to the increased convective energy loss from the flow of air around the fiber. Once the filament is free from the influence of the chamber, the profile resumes an exponential decay, the difference being the shift in the profile to a lower temperature throughout the remaining threadline, as compared with the threadline where no quench is employed.

Another important parameter in the quenching of the threadline is the length of the quenching device. This parameter was explored by generating threadline profiles with a quench chamber of lengths 10 and 20 cm. In all experiments, the quench air temperature was held at a constant 25°C and at 200 ft/min flow rate.

At 6000 m/min, the longer quench chamber slightly increased the stress level. Figure 20 shows the effect to be only slight, but still with the quench chamber, the stress level was increased, regardless of length. The freeze point was also closer to the spinneret with the quench chambers, so the dynamics of the threadline are accelerated with the quenching device.

SUMMARY

A computer simulation must always be treated as a simulation, and the user must realize that the information generated by the computer is just an estimation of a physical process. The simulation is a

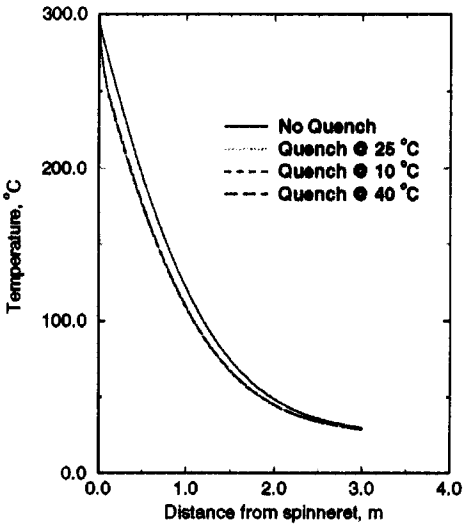

Figure 19 Temperature profiles comparing the effects of quench air temperature at 6000 m/min take-up, 0.6 IV polymer.

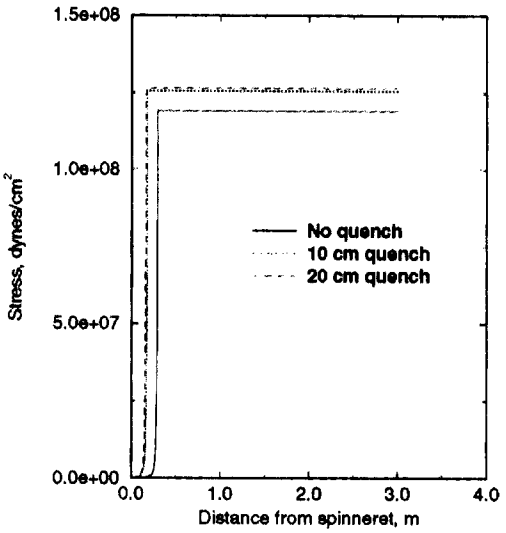

Figure 20 Stress profiles comparing the effects of quench chamber length at 6000 m/min take-up, 0.6 IV polymer.

research tool to be used to supplement laboratory experimentation, not replace it. Such a tool can be very useful in exploring situations that may not be feasible in a laboratory, whether limitations lie with the equipment or with safety reasons. More importantly, the simulation can be used to conduct time-consuming optimization experiments, a major factor when incorporating threadline modifications into the traditional threadline.

Verification of the simulation with experimental data has led to several conclusions concerning the validity of the data generated by the computer. Diameter, velocity, and temperature compare favorably between the predicted and the measured values. The diameter profiles are not as good as the velocity and temperature profiles, but overall the calculated profiles agree closely with the experimental. Comparison with crystallinity and birefringence measurements made off-line on collected samples, however, point out deficiencies of the program in the prediction of these properties. Because the calculations are based on empirical relationships adapted from other work, this was somewhat expected. The great disparity between the program and the experimentally measured data at low IVs was not expected. Thus exploration of these relationships is warranted and caution is advised if the simulation is to be used for the prediction of crystallinity and birefringence under the circumstances where the preceding analysis has shown it to be questionable.

REFERENCES

1. J. Shimizu, N. Okui, and T. Kikutani, *High-Speed Fiber Spinning,* A. Ziabicki and Kawai, Eds., Wiley, New York, 1985, Chap. 7.
2. A. Ziabicki, *High-Speed Fiber Spinning,* A. Ziabicki and Kawai, Eds., Wiley, New York, 1985, Chap. 2.
3. M. Matsui, *Trans. Soc. Rheol.,* **20,** 465 (1976).
4. D. K. Gagon, Master's Thesis, University of Delaware, 1980.
5. F. Krieth, *Principles of Heat Transfer,* 2nd ed., International Textbook Co., Scranton, PA, 1965, p. 595.
6. S. Kase and T. Matsuo, *J. Polym. Sci.,* **A3,** 2541 (1965).
7. S. Kase and T. Matsuo, *J. Appl. Polym. Sci.,* **11,** 251 (1967).
8. A. B. Metzner, *Processing of Thermoplastic Materials,* E. C. Bernhardt, Ed., Reinhold, New York, 1959, Chap. 1.
9. N. Phan-Thien, *Trans. Soc. Rheol.,* **22,** 259 (1978).
10. M. Yamamoto, *J. Phys. Soc. Jpn.,* **11,** 413 (1956).
11. M. Yamamoto, *J. Phys. Soc. Jpn.,* **12,** 1148 (1957).
12. M. Yamamoto, *J. Phys. Soc. Jpn.,* **13,** 1200 (1958).
13. A. S. Lodge, *Kolloid-Z.,* **171,** 46 (1960).
14. A. S. Lodge, *Rheol. Acta,* **7,** 379 (1968).
15. A. Ziabicki and L. Jarecki, *High-Speed Fiber Spinning,* A. Ziabicki and Kawai, Eds., Wiley, New York, 1985 Chap. 9.
16. H. H. George, *High-Speed Fiber Spinning,* A. Ziabicki and Kawai, Eds., Wiley, New York, 1985, Chap. 10.
17. R. Murray, H. A. Davis, and P. Tucker, *J. Appl. Polym. Sci.,* **33,** 177 (1978).
18. G. Perez, *High-Speed Fiber Spinning,* A. Ziabicki and Kawai, Eds., Wiley, New York, 1985, Chap. 12.
19. J. M. Schultz, *Polym. Eng. Sci.,* **31,** 661 (1991).
20. K. Fujimoto, K. Iohara, S. Ohwaki, and Y. Murase, *J. Appl. Polym. Sci.,* **42,** 1509 (1991).
21. H. Yasuda, H. Sugiyama, and H. Yanagawa, *Sen-l Gakkaishi,* **35,** T-370 (1979).
22. C. Bai, Ph.D. Thesis, University of Tennessee, 1986.
23. K. Katayama and M. Yoon, *High-Speed Fiber Spinning,* A. Ziabicki and Kawai, Eds., Wiley, New York, 1985, Chap. 8.
24. K. Nakamura, K. Katayama, and T. Amano, *J. Appl. Polym. Sci.,* **17,** 1031 (1973).
25. K. Katayama and M. Yoon, *High-Speed Fiber Spinning,* A. Ziabicki and Kawai, Eds., Wiley, New York, 1985, Chap. 8.
26. I. M. Hamana, M. Matsui, and S. Kato, *Melliand Text. Berich.,* **50,** 382 (1969).
27. C. Y. Lin, Ph.D. Thesis, North Carolina State University, 1990.

Received August 30, 1994
Accepted January 31, 1995